

# Transient Thermal Analysis of Human Exposure to Electromagnetic Fields

Abdelmalek Laissaoui<sup>1, \*</sup>, Ammar Abdi<sup>1</sup>, Sabrina Mezoued<sup>1</sup>,  
Bachir Nekhou<sup>2</sup>, and Dragan Poljak<sup>3</sup>

**Abstract**—The study of the thermal effect caused by exposure to electromagnetic fields is a focus of this research. To quantify the induced current and temperature distribution in the human body an assessment tool for the frequency range of 50 Hz to 110 MHz has been developed. The major contribution consists of providing a quantitatively accurate and relatively simple model. The formulation of the problem is based on a simplified cylindrical representation defined by the anatomical parameters of the human body. The bio-thermal modeling is carried out in two stages. Firstly, the electromagnetic analysis is based on the transmission lines (TL) theory. Secondly, a thermal modeling based on the thermal networks model (nodal method) is approached. This allows us to quantify the corresponding thermal gradients in the human body.

## 1. INTRODUCTION

Nowadays, electromagnetic waves are omnipresent in our environment because of their use in different fields of application (telecommunications, medicine, industry, etc.). This development of electromagnetic sources has led to an increase in the number of exposed users and raises several questions about the possible effects of these waves. Several studies providing some answers have been carried out to be able to limit exposure to electromagnetic radiation in order to provide protection against these effects. So far, all these studies consider that the only effects of electromagnetic waves in the frequency band of 100 kHz–100 GHz are thermal effects due to the power absorbed by the tissues which can cause a localized or widespread increase in temperature to a region. This tissue heating is characterized by the specific absorption rate (SAR) expressed in W/kg.

Basic electromagnetic field (EMF) exposure restrictions have been established by the International Commission on Non-Ionizing Radiation Protection (ICNIRP) [1] and IEEE [2] to verify compliance with these limits. Indeed, ICNIRP considers that the first effects appear from a SAR threshold equal to 4 W/kg for the whole body for RF field exposures in the 100 kHz to 6 GHz frequency range [2], which corresponds to a temperature rise of 1°C. From this threshold, they apply a safety factor of 10 to obtain the limit of 0.4 W/kg for workers and a factor of 50 to obtain the limit of 0.08 W/kg for the public. These reduction factors are introduced to take into account the scientific uncertainties linked to experimental errors for example.

In parallel with experimental dosimetry [3, 4], many scientific research teams have approached a new research field which is numerical dosimetry to quantify by calculating the interaction of electromagnetic fields with humans [5–8]. All this work was carried out either by experimental dosimetry using animals or artificial models (phantoms) of electrically representative whole or fragmentary bodies of different

---

*Received 24 April 2022, Accepted 22 June 2022, Scheduled 27 July 2022*

\* Corresponding author: Abdelmalek Laissaoui (laissaoui.abdelmalek@yahoo.fr).

<sup>1</sup> LSEL-Université des Sciences et Technologie Houari Boumediene, BP No. 32, Alger 16111, Algeria. <sup>2</sup> LAMEL Laboratory, University of Jijel, BP 98 OuledAissa 18000 Jijel, Algeria. <sup>3</sup> Faculty of Electrical Engineering, Mechanical Engineering and Naval Architecture, University of Split, R. Boskovicica 32, HR-21000 Split, Croatia.

morphologies or by numerical dosimetry based on anatomical models or homogeneous geometric models (cylinders, spheres, or ellipses) of the human body.

This article deals with an extension of the work reported in [9] by proposing electromagnetic-thermal modeling of the human body exposed to high frequency fields (HF). This realistic formalism and simple implementation with short computing times enabled us to access by calculation, for different sources of the EMF (constant or transient field), the induced current and the temperature distribution in the human body with an acceptable precision compared to the results obtained with more rigorous numerical modeling but rather cumbersome computer implementation.

By adopting a weak coupling of electromagnetic and thermal co-simulation, the electromagnetic model based on the transmission lines (TL) theory [10–12] will be weakly coupled to the thermal model based on the thermal network model, thus allowing us to obtain the evolution of the temperature in the human body. The dissipated power calculated through EM simulation becomes the heat source in the thermal simulation.

The approach thus developed from the theory of (TL) is reasonably accurate for the cylindrical model of the body [13]. This makes it possible to study the temporal response of humans illuminated by an electromagnetic wave. Once the distribution of the induced current along the body is obtained, one can then easily calculate the total power absorbed inside the body, the latter representing the source term of the thermal equation. Finally, the temperature rise induced by this exposure can be analyzed by solving the bio-heat transfer equation via the nodal method [14, 15]. By using this method, an equivalent thermal network of the cylindrical antenna model of the human is established. The comparison of the results obtained by the adopted approach with the numerical results obtained by the COMSOL Multiphysics software allowed us to validate our estimation tool.

This paper is organized as follows. Section 2 describes the simplified model of the body represented by a vertical cylinder used to evaluate human electro-thermal response to an electromagnetic wave for adult male and female models. Section 3 presents a new concept, developed from transmission lines for quantifying the electromagnetic phenomena induced in the human body, and the results. The thermal modeling of the human body using the nodal method based on equivalent thermal networks and results are presented in Section 4. Finally, Section 5 presents our conclusions.

## 2. ELECTROMAGNETIC MODELS OF HUMAN BODY

For the quantification of the energy induced in the human body illuminated by an EMF, the geometry commonly adopted to model the human body is that presented in Figure 1 [5]. The human body assumed to be homogeneous is represented by a vertical cylinder of height  $L$  and radius  $a$  perpendicular to a ground plane with arms in contact with the sides.

The human equivalent antenna has been originally proposed for experimental dosimetry and is valid within the frequency range from 50 Hz to 110 MHz, such as: the radius  $a$  of the conductor is small compared to its height ( $a \ll L$ ), and the minimum wavelength  $\lambda_{\min}$  is very large compared to the radius of the conductor ( $\lambda_{\min} \gg a$ ). Living matter has very special electrical properties, and in any case very different from conventional electrical engineering materials. These values of the electrical properties can vary a lot depending on field strength and frequency.

In the perspective of estimating the temperature distribution inside the human body in the case of exposure to a vertically polarized plane wave, the parameters of the equivalent cylindrical antenna were defined according to the anatomical parameters of the human body to model. Assuming the homogeneous body composed of muscular tissue, the anatomical parameters of the cylinder were defined in [16] as:

$$a = L_1 \sqrt{\frac{W}{\pi \rho_m L}} \quad (1)$$

$$h = L \quad (2)$$

$$\sigma_\omega = L_2 \frac{2x}{3-x} \sigma_{mus} \quad (3)$$

$$\rho = L_3 \frac{\rho_m}{x} \quad (4)$$

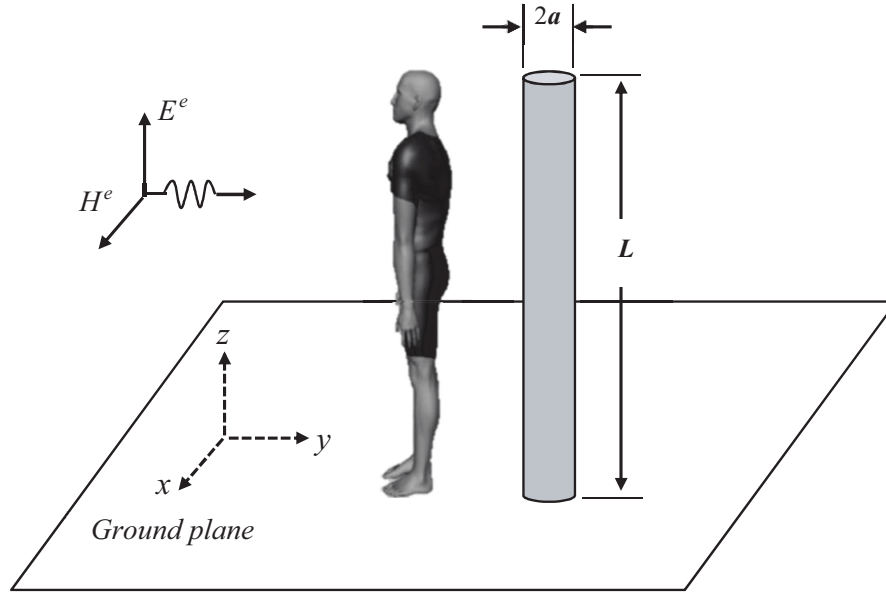


**Figure 1.** The cylindrical antenna model of the human body exposed to vertically polarised plane wave.

where  $W$  is the weight of the human subject [kg];  $L$  is the height [m];  $\rho_m$  is the average density [ $\text{kg m}^{-3}$ ];  $\sigma_{mus}$  is the complex electric conductivity of muscle [ $\text{S m}^{-1}$ ] defined in [16] ( $\sigma_{mus} = j\omega\epsilon_0\epsilon_{mus} = \sigma + j\omega\epsilon_0\epsilon_r$ , with  $\sigma$  being the electric conductivity of muscle [ $\text{S m}^{-1}$ ] and  $\epsilon_r$  the relative permittivity of muscle);  $\rho$  is the density [ $\text{kg m}^{-3}$ ];  $L_1$ ,  $L_2$ , and  $L_3$  are the constants of proportionality depend on the gender and age of the human subject; and  $x$  is a function of the lean body-mass of the human subject which was defined in [16]. The dimensions are given in Table 1.

**Table 1.** Geometric parameters [16].

| Adult males                                      | Adult females                                    |
|--|--|
| $x = 0.321 + \frac{1}{W}(33.92 \cdot L - 29.53)$ | $x = 0.295 + \frac{1}{W}(41.81 \cdot L - 43.29)$ |

### 3. CONCEPT OF TRANSMISSION LINE THEORY

This method is based on solving two differential equations (Telegraph equations) that describe the voltage and current on a transmission line. The pair of equations describing the coupling between a TL ( $n$  conductors) and an external EMF is given as follows [12]:

$$\frac{d[U(z, \omega)]}{dz} + [Z][I(z, \omega)] = [U_F(z, \omega)] \tag{5}$$

$$\frac{d[I(z, \omega)]}{dz} + [Y][U(z, \omega)] = [I_F(z, \omega)] \tag{6}$$

where  $[U(z, \omega)]$  and  $[I(z, \omega)]$  are  $n$  order complex vectors of total voltage and current along the transmission line;  $[Z]$  and  $[Y]$  are square matrices of order  $n$ , impedance and admittance per unit length complex. The expressions of the linear longitudinal impedance  $[Z]$  and admittance per unit length transverse  $[Y]$  used in this study are documented in detail in [11–17].  $[U_F(z, \omega)]$  and  $[I_F(z, \omega)]$  are complex vectors due to any external electromagnetic field and are defined as:

$$[U_F(z, \omega)] = -\frac{\partial}{\partial z} [E_T^e(z, \omega)] + [E_L^e(z, \omega)] \tag{7}$$

$$[I_F(z, \omega)] = -[Y][E_L^e(z, \omega)] \quad (8)$$

where  $[E_T^e(z, \omega)]$  are the sources due to incident transverse electric field, and  $[E_L^e(z, \omega)]$  are the sources due to incident longitudinal electric field.

In this study, we are only interested in the vertical (longitudinal) incident electric field to the human body. This vertical field  $E_z^e$  is the main cause of the energy absorption, and the dominant direction of the induced currents and voltages is also vertical (axial). By remaining within the fundamental assumptions of TL, the voltages and currents induced along the cylindrical antenna model of the human body can be calculated by solving the TL equations in the frequency domain. The technique used to solve the TL equations is well documented in our previous study [8].

The contact of the human body with the ground can be taken into account via a capacitance  $C$  [5]:

$$Z_0 = \frac{1}{j\omega C} \quad (9)$$

where  $C$  is the capacity between the sole of the foot and its image in the ground ( $C = (\pi a^2 \varepsilon_0 \varepsilon_{rs})/d$ );  $\varepsilon_{rs}$  is the relative permittivity of the material constituting the sole of the shoe;  $d$  is the distance between the sole of the shoe and its image in the ground. The second end of the human is connected by an impedance of great value, i.e.,  $Z_L = \infty$ .

### 3.1. Induced Axial Current in the Cylindrical Model

To calculate the induced axial current in the cylindrical model, the human body standing on a highly conductive infinite plane is illuminated by a vertically polarised plane wave with electric field parallel to the axis of the  $z$ -directed cylinder. A validation of our approach by a comparison of our results with those obtained by Poljak [18] by solving the Hallen equation in the time domain with the method of boundary elements of Galerkin-Bubnov (BEM-GB) is given in our previous study [9].

Assuming the impedance at the base of the cylinder  $Z_0 = 0 \Omega$ , Figures 2(a) and 2(b) respectively show the distribution of the induced current ( $I_z$ ) along the human body resulting from our calculations for adult male and female models with an incident electric field  $E_z^{inc}$  of 1 V/m at a frequency of 40 MHz.

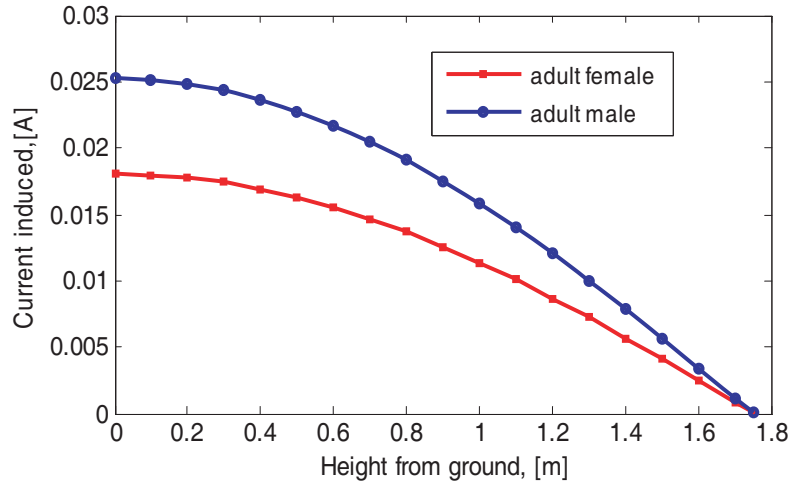


**Figure 2.** Axial current distribution induced in a human for adult male and female models,  $E_z^{inc} = 1 \text{ V/m}$ ,  $f = 40 \text{ MHz}$ .

The calculations are done considering that the electrical conductivity of the human body is of the order of  $\sigma = 0.67 \text{ S/m}$ , the relative permittivity  $\varepsilon_r$  equal to 82.7 for muscle tissue, and the average density approximately  $\rho' = 1000 \text{ kg m}^{-3}$  ( $f = 40 \text{ MHz}$ ) [19]. In Table 2, the constants of proportionality ( $L_1$ ,  $L_2$  and  $L_3$ ) are recorded according to gender taken from [16]. From Figure 2, we can see that the current induced in the human body ( $I_z(z)$ ) is significant at the level of the feet. From there, it gradually decreases until it becomes zero at the level of the head and that the responses of the adult

**Table 2.** Geometric parameters and constants of proportionality.

|              | <b>W</b> | <b>L</b> | <b>L<sub>1</sub></b> | <b>L<sub>2</sub></b> | <b>L<sub>3</sub></b> |
|--------------|----------|----------|----------------------|----------------------|----------------------|
| Adult male   | 75 kg    | 1.75     | $\sqrt{5}$           | 0.25                 | 0.38                 |
| Adult female | 58 kg    | 1.6      | $\sqrt{5}$           | 0.21                 | 0.44                 |

male and female models are comparable in general appearance with a slight difference in amplitude, and peak currents of 0.0252 A and 0.0153 A were calculated in the feet for the adult male and female models, respectively.

Knowledge of the current distribution allows us to determine the total average power dissipated  $P_{av}$  and the induced electric field  $E_z$  inside the cylinder. The total average power dissipated  $P_{av}$  can be written as [16]:

$$P_{av} \cong \frac{1}{2} R_L \int_0^L |I_z(z)|^2 dz \quad (10)$$

and the electric field inside the human body is given by [20]:

$$E_z(\rho, z) = \frac{J_z(\rho, z)}{\sigma + j\omega\epsilon} \quad (11)$$

where  $R_L$  is the real part of total impedance  $[Z]$  per unit length, which represents the power dissipated inside the human body due to ohmic losses of the body, and  $J_z(\rho z)$  is the current density induced in the body given by [8].

For the whole body averaged SAR (WBA-SAR) useful for estimating elevations of the core body temperature, one can use the following definition [16]:

$$SAR_{(WBA)} = \frac{P_{av}}{W} \quad (12)$$

where  $P_{av}$  is the total average power dissipated,  $\rho$  the mass density  $[\text{kg m}^{-3}]$ , and  $W$  the weight of the human subject  $[\text{kg}]$  ( $W = \rho\pi a^2 L$ ).

The results for the average power dissipated in the human body and the whole body averaged SAR are shown in Table 3. We can notice that the values of the average power dissipated are very weak.

**Table 3.** Results of the exposure.

|                     | <b>P<sub>av</sub> [mW]</b> | <b>SAR<sub>(WBA)</sub> [<math>\mu\text{W}/\text{kg}</math>]</b> |
|---------------------|----------------------------|---|
| <b>Adult male</b>   | 10.214                     | 30.238  |
| <b>Adult female</b> | 5.980                      | 20.062  |

#### 4. TEMPERATURE DISTRIBUTION IN THE HUMAN BODY

Thermal behavior in living organisms has been analytically modeled by Pennes [21] through the transient bioheat equation presented below (the indices  $m$  and  $b$  refer to the medium and blood, respectively):

$$\rho_m C_m \frac{\partial T}{\partial t} = \vec{\nabla} \cdot (K_t \vec{\nabla} T) + \rho_b C_b \omega_b (T_b - T) + Q_{met} + Q_{EM} \quad (13)$$

where  $C_m$  is the specific heat of the tissue  $[\text{J kg}^{-1}\text{C}^{-1}]$ ,  $\rho_m$  the density of the tissue  $[\text{kg m}^{-3}]$ ,  $K_t$  the thermal conductivity of the tissue  $[\text{W m}^{-1}\text{C}^{-1}]$ ,  $t$  the continuous times  $[\text{s}]$ ,  $T$  the tissue temperature  $[\text{C}^\circ]$ ,  $\omega_b$  the blood flow rate  $[\text{kg m}^{-3} \text{s}^{-1}]$ ,  $C_b$  the specific heat of blood  $[\text{J Kg}^{-1}\text{C}^{-1}]$ ,  $\rho_b$  the density of blood  $[\text{kg m}^{-3}]$ ,  $T_b$  the temperature of blood  $[\text{C}^\circ]$ ,  $Q_{met}$  the heat produced by the metabolism  $[\text{W m}^{-3}]$ , and  $Q_{EM}$  ( $Q_{EM} = \rho_m \text{ SAR}$ ) is the heat produced by the electromagnetic field per unit volume  $[\text{W m}^{-3}]$ .

These heat exchange processes which ensure the maintenance of the thermal equilibrium are the following: generation of thermal energy inside the tissue by metabolism, energy transfer by thermal conduction, energy transfer by convection, and storage of energy by the tissue during the transient regime. In this analysis, the contribution of cooling effect of blood ( $\rho_b C_b \omega_b (T_b - T)$ ) is not taken into account, is weaker since the body temperature is near the ambient temperature [22], and the metabolic heat generation  $Q_m$  is assumed zero in the analysis, as we seek to assess the thermal effect of electromagnetic energy associated with exposure.

The thermal modeling of the human body model will be approached using the nodal method based on equivalent thermal networks which takes into account the different transfers of heat.

#### 4.1. Equivalent Transient Thermal Network of the Human Body Model

This modeling method [14, 15] consists of reducing the study of the thermal behavior to an equivalent electrical diagram using resistors and thermal capacities. The principle of the nodal method is to discretize the cylindrical model of the human body into a certain number of elementary volumes ( $\Omega_i$ ) of cylindrical shapes. A cylindrical element, its dimensions and its temperatures, given by Figure 3 is used as a basis to model the human body.

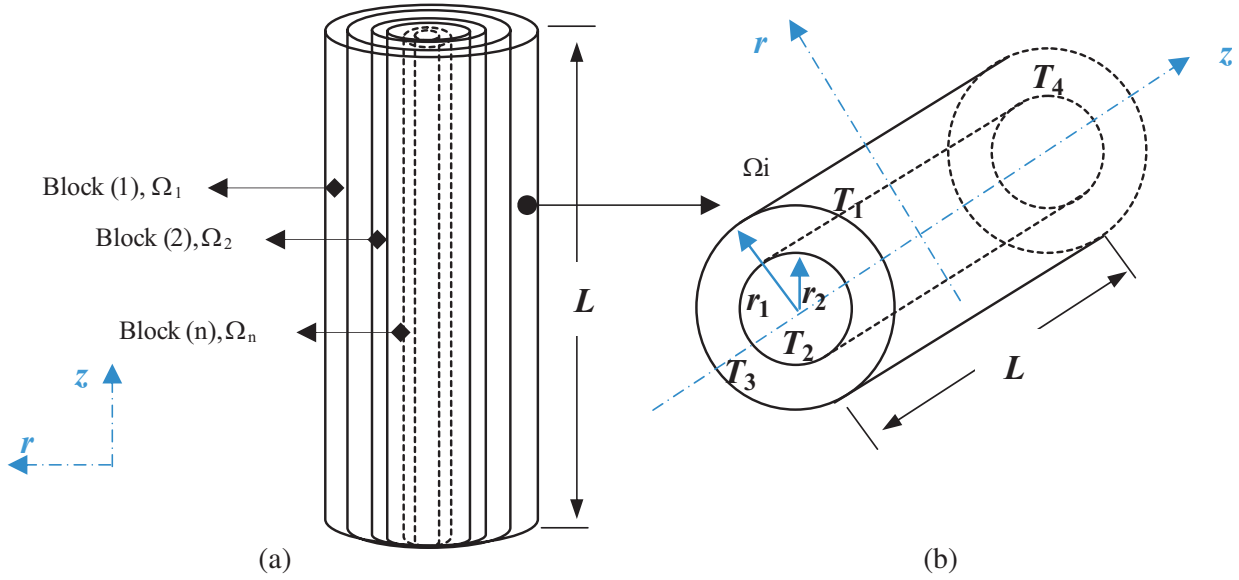


**Figure 3.** (a) Nodal discretization of the human body model. (b) Representation of an elementary block with cylindrical bidirectional with four unknown temperatures: two at the axial edges and two on the outer and inner surfaces.

The thermo-physical properties of each elementary volume are assumed to be concentrated in the center of the volume. Each node is characterized by three thermal parameters: its electromagnetic heat-source ( $P_i$ ), its heat capacity ( $C_i$ ), and its temperature ( $T_i$ ). The nodes of each volume are linked by thermal conductance describing the nature of the heat transfer between the nodes.

After discretization of the system into nodes, the energy balance in each node makes it possible to have the algebro-differential system of Equation (14) [14, 15–23]. Equation (13) can therefore be rewritten:

$$C_i \frac{dT_i}{dt} = \sum_{j=1}^n G_{ij} (T_j - T_i) + P_i \quad (14)$$

where  $C_i = \rho_{mi} C_{pi} \Omega_i$  is the heat capacity of node  $i$ ;  $\rho_{mi}$ ,  $C_{pi}$ ,  $\Omega_i$  are respectively the density, specific heat, and volume from block  $i$ ;  $P_i$  is the electromagnetic heat-source at node  $i$ ;  $G_{ij}$  is the transfer conductance between nodes  $i$  and  $j$ ;  $n$  is the number of nodes linked to node  $i$ .

Writing Equation (14) through all the nodes of the global volume to be modeled leads us to a set of differential equations which is written in matrix form as

$$[C] \left\{ \frac{dT}{dt} \right\} = [G] \{T\} + \{P\} \tag{15}$$

where  $[C]$  is the diagonal matrix of thermal capacities,  $[G]$  the matrix of thermal conductance describes all the modes of heat transfer,  $\{T\}$  the temperature vector, and  $\{P\}$  the electromagnetic heat-source vector.

For a 2D study in the  $(r, z)$  plane (Figure 3(b)), the resolution of the differential equations of transfer in the two radial and axial directions makes it possible to obtain a distribution of the temperature in the human body. Thus, the establishment of an equivalent thermal circuit is possible; this with the following assumptions: the heat flows in the axial, and radial directions are independent. The same average temperature defines the flow in the axial and radial direction, and no circumferential heat flow and the thermal conductivity in the axial and radial directions are identical.

4.1.1. Circuit of the Elementary Block in the Axial Direction

For a cylinder, the steady state heat conduction in the axial direction is governed by the Poisson Equation (16), as

$$k_z \frac{d^2T}{dz^2} + Q_{EM} = 0 \tag{16}$$

where  $k_z$  is the thermal conductivity in the axial direction;  $Q_{EM}$  is the volumic power density (electromagnetic heat-source). If it is assumed that the temperatures in the cylinder are symmetrical about a central radial plane so that the temperatures  $T_3$  and  $T_4$  are equal, the equivalent thermal circuit is shown schematically in Figure 4(b). The used expressions of the different resistances can be defined as reported in Table 4 [24].

**Table 4.** The elements of the elementary block in the axial and radial directions [24].

| Elementary block in the axial direction   | Elementary block in the radial direction       |  |
|---|--|--|
| $R_{zms} = \frac{R_0}{6} = \frac{L}{6 \cdot \pi \cdot K_z (r_1^2 - r_2^2)}$<br>$R_0 = \frac{L}{\pi \cdot K_z (r_1^2 - r_2^2)}$<br>$R_0$ is the thermal resistance in the axial direction, it is given by the expression | $R_{r1} = \frac{1}{2\pi k_r L}$                | $1 - \frac{2r_2^2 \ln\left(\frac{r_1}{r_2}\right)}{(r_1^2 - r_2^2)}$                   |
|   | $R_{r2} = \frac{1}{2\pi k_r L}$                | $\frac{2r_1^2 \ln\left(\frac{r_1}{r_2}\right)}{(r_1^2 - r_2^2)} - 1$                   |
|   | $R_{rm} = \frac{-1}{4\pi(r_1^2 - r_2^2)k_r L}$ | $r_1^2 + r_2^2 - \frac{4r_1^2 r_2^2 \ln\left(\frac{r_1}{r_2}\right)}{(r_1^2 - r_2^2)}$ |

4.1.2. Circuit of the Elementary Block in the Radial Direction

Heat transfer by conduction in the radial direction is governed by the equation of Poisson in one dimension, which is written as

$$k_r \frac{d^2T}{dr^2} + k_r \frac{1}{r} \frac{dT}{dr} + Q_{EM} = 0 \tag{17}$$

where  $k_r$  is the thermal conductivity in the radial direction.

The solution of Equation (17) makes it possible to establish the equivalent thermal circuit. The elements of the equivalent circuit described in Figure 4(a) are defined in Table 4 [24].

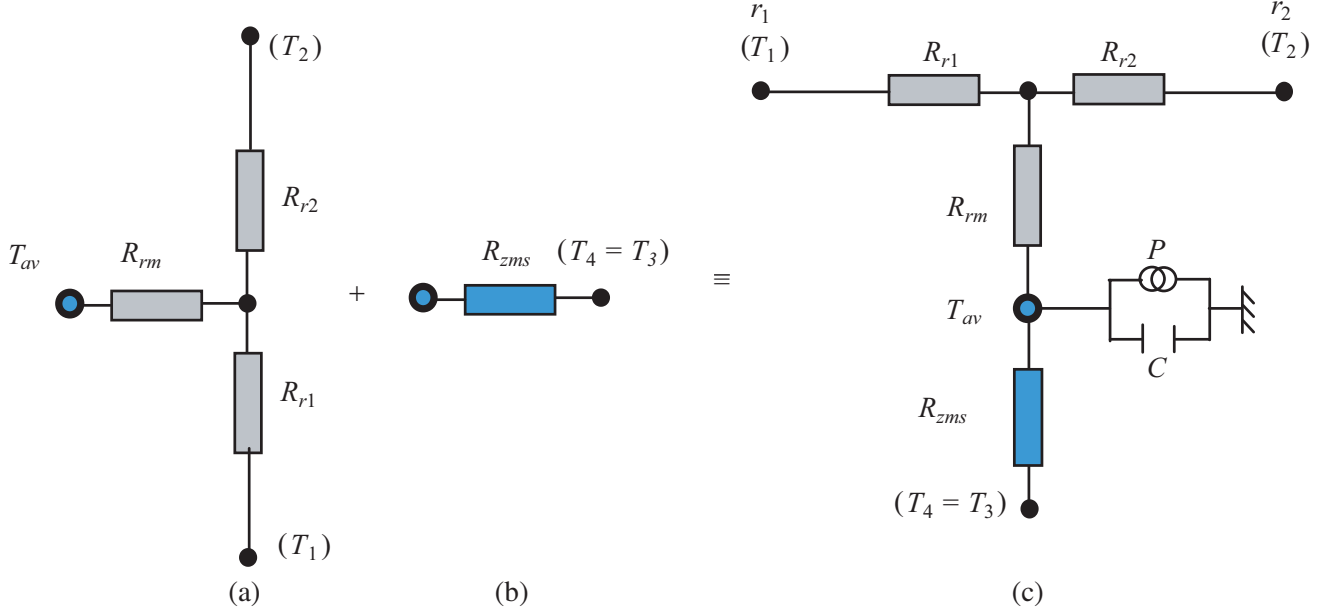


**Figure 4.** Equivalent thermal circuit (a) in the radial direction and (b) in the axial direction, (c) combined thermal network for symmetric component.

#### 4.1.3. Global Elementary Block Circuit

Obtaining a simple elementary network of this model can be done by combining the two elementary networks of Figure 4(a) and Figure 4(b), and the combination of these two elementary networks leads to the elementary network shown in Figure 4(c) [24]. The electromagnetic heat-source (power) will be considered by connecting it to the medium temperature node as a flux source thermal. This power is defined by  $P_i = \iiint_{\Omega_i} Q_{EM} d\Omega_i$ . In order to study the thermal transients, the thermal capacity of the

block is also injected at the level of the central node.

The thermal resistance corresponding to the exchange at the air–human body interface (convective cooling) is [24]:

$$R_{cra} = \frac{1}{hS} \quad (\text{convection resistance}) \quad (18)$$

where  $h$  is the convection coefficient [ $\text{W m}^{-2} \text{C}^{-1}$ ] ( $h = 5 \text{ W m}^{-2} \text{C}^{-1}$ ), and  $S$  is the surface in contact with the air [ $\text{m}^2$ ].

The equivalent thermal network that corresponds to the geometric model of the human body and the boundary conditions for heat transfer are shown in Figure 5. The equivalent nodal network is obtained by cutting the model of the human body into  $n_t = 50$  elementary blocks in radial direction (nodes at average temperatures). Each elementary block is described by its equivalent circuit, and the air-human body interface is described by a convection thermal resistance.

#### 4.1.4. Equation of the Thermal Model

The model equations are then grouped into two systems whose forms are as follows:

$$[C] \left\{ \frac{dT_{av}}{dt} \right\} + [G_{11}] \{T_{av}\} + [G_{12}] \{T\} = \{P\} \quad (19)$$

$$[G_{21}] \{T_{av}\} + [G_{22}] \{T\} = 0 \quad (20)$$

where  $[C]$  is the diagonal matrix of heat capacities of dimension  $(n_t \times n_t)$ ,  $n_t$  the number of solid element,  $[G_{11}]$  the thermal conductance matrix of dimension  $(n_t \times n_t)$ ,  $[G_{12}]$  the thermal conductance matrix of dimension  $(n_t \times (n_t - 1))$ ,  $[G_{22}]$  the thermal conductance matrix of dimension  $((n_t - 1) \times (n_t - 1))$ ,

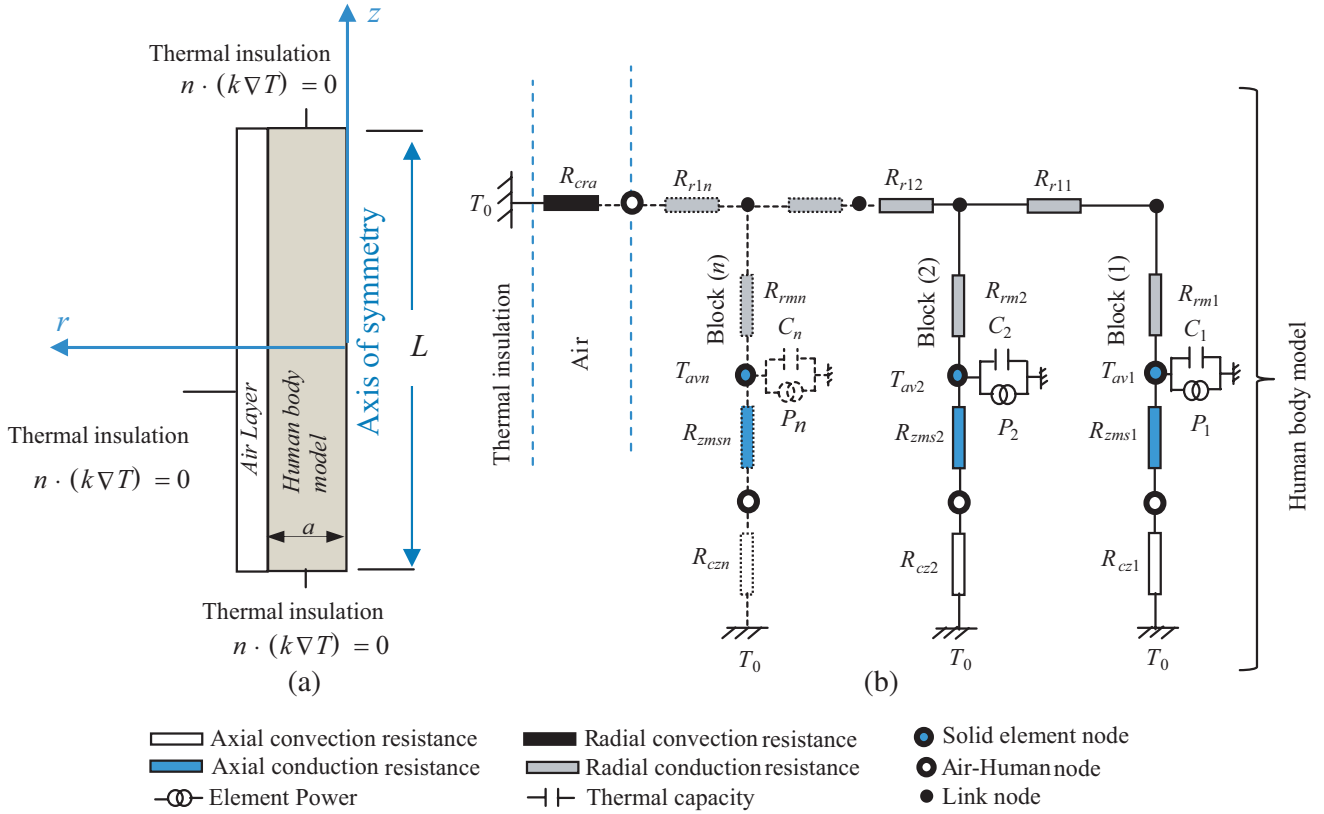


**Figure 5.** (a) Boundary conditions for heat transfer, (b) equivalent thermal network of the model of human body.

$[G_{21}]$  the transpose matrix of  $[G_{12}]$ ,  $\{T_{av}\}$  the vector of average temperatures,  $\{T\}$  the vector of the temperatures of the connection nodes, and  $\{P\}$  the vector of electromagnetic heat-source.

The systems (19) and (20) lead to a differential system of the form

$$[C] \left\{ \frac{dT_{av}}{dt} \right\} + [G] \{T_{av}\} = \{F\} \quad (21)$$

where  $[G] = [C]^{-1}([G_{11}] - [G_{12}][G_{22}]^{-1}[G_{21}])$  and  $\{F\} = [C]^{-1}\{P\}$ .

In order to determine the evolution of temperatures in the model of the human body, a program under MATLAB has been developed to solve the system (21), using Runge Kutta's method.

### 4.2. Results and Validation

By exploiting the thermal model of the human body developed, an analysis of the temperature distribution in the equivalent cylindrical antenna model of the humans parameterized as adult males and females is presented in this section. We give the results describing the most significant quantities in the thermal point of view.

In order to predict the thermal distribution in the human body, the ambient temperature is taken at  $37^\circ\text{C}$ , and the initial temperature of the body is  $37^\circ\text{C}$ .

Figures 6(a) and 6(b) show the time evolution of temperature rise  $\Delta T$  (with:  $\Delta T = T - T(t_0)$ ) at a fixed point on the surface of the body model, for adult male and female models respectively, after 35 minutes of exposure (adult male:  $z = 0.875\text{ m}$ ,  $a = 0.26\text{ m}$ , adult female:  $z = 0.8\text{ m}$ ,  $a = 0.24\text{ m}$ ), for  $f = 40\text{ MHz}$ ,  $\rho_m = 1000\text{ kg m}^{-3}$ ,  $K_t = 0.5\text{ W m}^{-1}\text{C}^{-1}$  and  $C_m = 3650\text{ J kg}^{-1}\text{C}^{-1}$ . At  $f = 40\text{ MHz}$ , the results of the thermal model are compared with those obtained numerically by COMSOL software based on the finite elements method (FEM). One notes that a good estimation of the temperature is obtained between our calculation results and that using the COMSOL Multiphysics software.

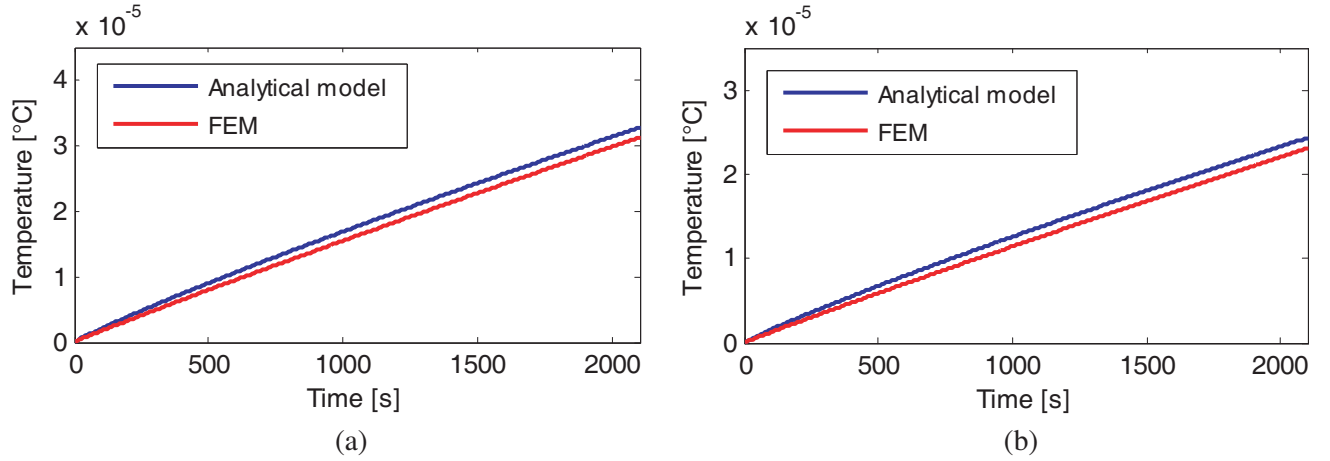


**Figure 6.** Temperature rise  $\Delta T$  at the surface of the adult (a) male model ( $z = 0.875$  m,  $a = 0.26$  m) and (b) female model ( $z = 0.8$  m,  $a = 0.24$  m) for  $f = 40$  MHz.

In order to better complete the comparison between the results from our modeling and those provided by the COMSOL software, we propose a statistical analysis of the results. For this, we calculate the RMSE (root mean square error) [25]. The values obtained were  $1.3204 \cdot 10^{-6} \text{ } ^\circ\text{C}$  and  $1.0740 \cdot 10^{-6} \text{ } ^\circ\text{C}$  respectively for adult male and female models. The differences in the results are acceptable taking into account different solution methods. This last observation confirms our modeling and our calculation results.

The result confirms that the temperature rise in the adult male model is higher than that of the adult female model. It therefore seems that the morphology of the subject has an influence on the rise in temperature. The maximum rises in temperature as calculated for adult male and female models after 35 minutes of exposure with this method were approximately  $\Delta T = 3.27 \cdot 10^{-5} \text{ } ^\circ\text{C}$  and  $\Delta T = 2.428 \cdot 10^{-5} \text{ } ^\circ\text{C}$ , respectively, which seems rather negligible. This result suggests that exposure does not significantly alter human body temperature in the case of 40 MHz frequency.

Figures 7(a) and 7(b) show respectively the temperature rise  $\Delta T$  in the feet and at the level of the head for the adult male and female models at  $f = 40$  MHz. We find that the temperature rises for the two positions and at the different models have almost the same magnitude and are negligible because the rise is mainly a local phenomenon.

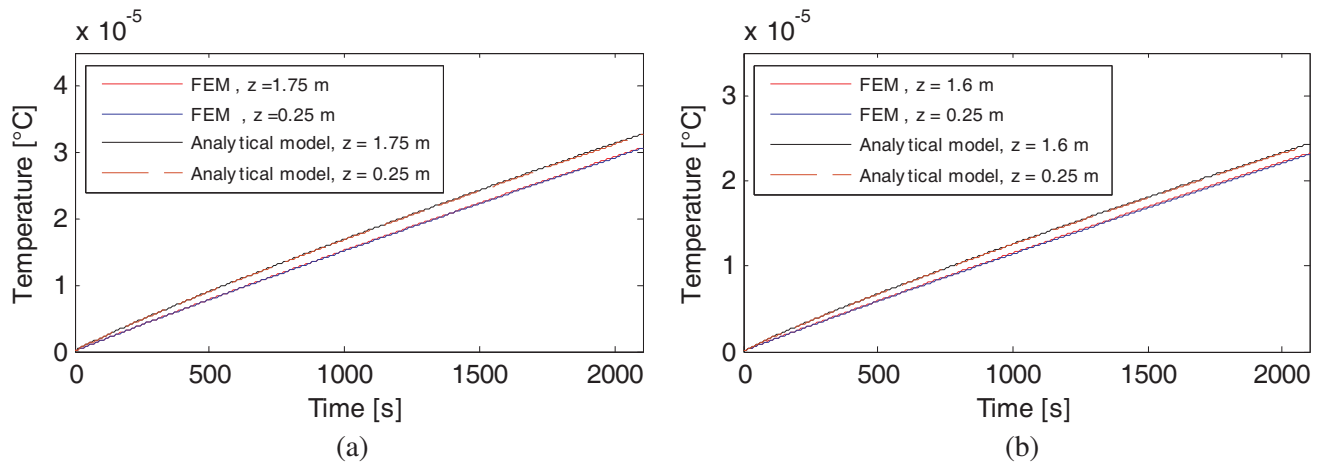


**Figure 7.** Temperature rise  $\Delta T$  at the surface of the adult (a) male model ( $z = 0.25$  m and  $z = 1.75$  m,  $a = 0.26$  m) and (b) female model ( $z = 0.25$  m and  $z = 1.6$  m,  $a = 0.24$  m) for  $f = 40$  MHz.

## 5. CONCLUSION

In this article, the electromagnetic-thermal model for human exposure to electromagnetic fields in the frequency rang of 50 Hz to 110 MHz is presented. The formulation is based on a simplified cylindrical representation of the human body.

In the first step, we have presented an electromagnetic modeling based on the theory of transmission lines which makes it possible to evaluate different electromagnetic quantities in the human body. Once the axial current distribution is obtained, it is possible to calculate the power absorbed inside the body, which constitutes the heat source of the thermal problem.

In the second step, a thermal model based on equivalent thermal networks allowed us to obtain the temperature distribution for different morphologies of the human body in transient state. Finally, to validate the developed calculations, the obtained results are satisfactorily compared with those obtained by the COMSOL Multiphysics commercial software based on the finite elements method. The comparison shows good agreement between the results, which makes it possible to validate the proposed model.

The advantage of the electromagnetic model based on the theory of transmission lines coupled with the thermal model based on the nodal method" approach is that it makes it possible to provide an easy, efficient, and non-prohibitive modeling in computing time compared to other more elaborate numerical methods with a good quality of results and contribute in a very remarkable way in the transient analysis of the electro-thermal response of the human body illuminated by electromagnetic field by avoiding the problem of instability of the results. Another advantage of this modeling is that it makes it possible to highlight certain parameters influencing the distribution of the induced current and the temperature profile, such as the effect of shoes, the conductivity of the ground, and the processes of heat exchange. The disadvantages of this approach lie in the fact that it does not allow the analysis of complicated structures and incorrect at a very high frequency range.

## REFERENCES

1. "ICNIRP 2020 Guidelines for limiting exposure to electromagnetic fields (100 kHz to 300 GHz)," *Health Phys.*, Vol. 118, No. 5, 483–524, ICRP 1975 Report of the Task Group on Reference Man Vol. 23, Pergamon, Oxford, 1975.
2. IEEE-C95.1 2019 IEEE Standard for Safety Levels with Respect to Human Exposure to Radio Frequency Electromagnetic Fields, 0 Hz to 300 GHz, IEEE, NY, USA.
3. Dogan, H., I. B. Basyigit, S. Ozen, and S. Helhel, "EMF exposure and SAR analysis in the cow tissues," *International Journal of Scientific Engineering and Science*, Vol. 1, No. 12, 15–18, 2017.
4. Helhel, S., S. Ozen, I. B. Basyigit, O. Kurnaz, Y. E. Yoruk, and M. Bitirgan. "Radiated susceptibility of medical equipment in health care units: 2G AND 3G mobile phones as an interferer," *Microwave and Optical Technology Letters*, Vol. 53, No. 11, 2657–2661, November 2011.
5. Poljak, D, and V, Roje, "Currents induced in human body exposed to the power line electromagnetic field," *Proceedings of the 20th Annual International Conference of the IEEE*, Vol. 6, 3281–3284, Engineering in Medicine and Biology Society, IEEE, 1998.
6. Zhang, H. H., et al., "Electromagnetic-thermal analysis of human head exposed to cell phones with the consideration of radiative cooling," *IEEE Antennas Wireless Propag. Lett.*, Vol. 17, No. 9, 1584–1587, September 2018.
7. Gandhi, O. P. and J. Chen, "Numerical dosimetry at power-line frequencies using anatomically based models," *Bioelectromagnetics*, Vol. 13, No. S1, 43–60, 1992.
8. Laissaoui, A., B. Nekhoul, K. Kerroum, K. El Khamlichi Drissi, and D. Poljak, "On the rotationally-cylindrical model of the human body exposed to elf electric field," *Progress In Electromagnetics Research M*, Vol. 29, 165–179, 2013.
9. Laissaoui, A., B. Nekhoul, S. Mezoued, and D. Poljak, "Assessment of the human exposure to transient and time-harmonic fields using the enhanced transmission line theory approach," *AUTOMATIKA*, Vol. 58, No. 4, 355–362, 2018.

10. Paul, C. R., *Analysis of Multiconductor Transmission Lines*, 641–692, Wiley Interscience, New York, NY, 1994.
11. Paul, C. R., “A spice model for multiconductor transmission lines excited by an incident electromagnetic field,” *IEEE Trans. Electromagnet. Compat.*, Vol. 36, No. 4, 342–354, 1994.
12. Taylor, C. D., R. S. Satterwhite, and C. W. Harrison, Jr., “The response of terminated two-wire transmission line excited by a non uniform electromagnetic field,” *IEEE Transactions on Antennas and Propagation*, Vol. 13, 987–989, 1965.
13. King, R. W. P. and S. S. Sandler, “Electric fields and currents induced in organs of the human body when exposed to ELF and VLF electromagnetic fields,” *Radio Science*, Vol. 31, No. 5, 1153–1167, 1996.
14. Bates, J. J. and A. Tustin, “Temperature rises in electrical machines as related to the properties of the thermal networks,” *Proceeding IEE*, Vol. 103, No. 11, 471–482, 1956.
15. Kotnik, R. L., “An equivalent thermal circuit for non-ventilated induction motors,” *Transactions AIEE*, Vol. 73, 1604–1609, 1954.
16. Kibret, B., A. K. Teshome, and D. T. H. Lai, “Cylindrical antenna theory for the analysis of whole-body averaged specific absorption rate,” *IEEE Transactions on Antennas and Propagation*, Vol. 63, No. 11, 5224–5229, November 2015.
17. Ametani, A., Y. Kasai, J. Sawada, et al., “Frequency dependent impedance of vertical conductors and a multiconductor tower model,” *IEE Proc. — Gener. Trans. Distrib.*, Vol. 141, No. 4, 339–345, 1994.
18. Poljak, D., “Average power and total energy absorbed in the human body exposed to transient fields,” *Proceedings of the 12th IEEE Mediterranean Electrotechnical Conference (MELECON)*, Vol. 2, 507–510, Dubrovnik, Croatia, May 12–15, 2004.
19. Dielectric Properties of the Body Tissues, <http://niremf.ifac.cnr.it/tissprop/htmlclie/htmlclie.htm>.
20. Poljak, D., C. Y. Tham, O. Gandhi, et al., “Human equivalent antenna model for transient electromagnetic radiation exposure,” *IEEE Trans. Electromagnet. Compact.*, Vol. 45, No. 1, 141–145, 2003.
21. Pennes, H. H., “Analysis of tissue and arterial blood temperatures in the resting human forearm,” *J. Appl. Phys.*, Vol. 85, No. 1, 5–34, July 1998.
22. Zhang, H. H., Y. Liu, X. Y. Z. Xiong, G. M. Shi, C. Y. Wang, and W. E. I. Sha, “Investigating thermal cooling mechanisms of human body under exposure to electromagnetic radiation,” *IEEE Access*, Vol. 7, 9697–9703, 2019.
23. Fan, J., C. Zhang, Z. Wang, Y. Dong, C. E. Nino, A. R. Tariq, and E. G. Strangas, “Thermal analysis of permanent magnet motor for the electric vehicle application considering driving duty cycle,” *IEEE Transactions on Magnetics*, Vol. 46, No. 6, 2493–2496, 2010.
24. Mellor, P. H., D. Roberts, and D. R. Turner, “Lumped parameter model for electrical machines of TEFC design,” *IEE Proceeding — B*, Vol. 138, No. 5, 205–218, September 1991.
25. Chai, T. and R. R. Draxler, “Root Mean Square Error (RMSE) or Mean Absolute Error (MAE) — Arguments against avoiding RMSE in the literature,” *Geoscientific Model Development*, Vol. 7, No. 3, 1247–1250, 2014.